Since January 2020 Elsevier has created a COVID-19 resource centre with free information in English and Mandarin on the novel coronavirus COVID-19. The COVID-19 resource centre is hosted on Elsevier Connect, the company's public news and information website.

BioSystems 196 (2020) 104184

Contents lists available at ScienceDirect

BioSystems

journal homepage: www.elsevier.com/locate/biosystems

Analysis of the initiation of viral infection under flow conditions with applications to transmission in feed

Vladimir P. Zhdanov [a,b,*], Joshua A. Jackman [c]

[a] Section of Biological Physics, Department of Physics, Chalmers University of Technology, S-41296 Göteborg, Sweden
[b] Boreskov Institute of Catalysis, Russian Academy of Sciences, Novosibirsk 630090, Russia
[c] School of Chemical Engineering, Sungkyunkwan University, Suwon 16419, Republic of Korea

ARTICLE INFO

Keywords:
Viruses
Infection
Kinetic models
Growth
Flow
Diffusion

ABSTRACT

While kinetic models are widely used to describe viral infection at various levels, most of them are focused on temporal aspects and understanding of corresponding spatio-temporal aspects remains limited. In this work, our attention is focused on the initial stage of infection of immobile cells by virus particles ("virions") under flow conditions with diffusion. A practical example of this scenario occurs when humans or animals consume food from virion-containing sources. Mathematically, such situations can be described by using a model constructed in analogy with those employed in chemical engineering for analysis of the function of a plug-flow reactor with dispersion. As in the temporal case, the corresponding spatio-temporal model predicts either the transition to a steady state or exponential growth of the populations of virions and infected cells. The spatial distributions of these species are similar in both of these regimes. In particular, the maximums of the populations are shifted to the upper boundary of the infected region. The results illustrating these conclusions were obtained analytically and by employing numerical calculations without and with the dependence of the kinetic parameters on the coordinate. The model proposed has also been used in order to illustrate the effect of antiviral feed additives on feedborne infection towards curbing disease transmission.

1. Introduction

The mechanisms of initiation and spread of viral infections are inordinately diverse and complex, and one of the ways to clarify them systematically is based on the development of theoretical models (Bocharov et al., 2018b; Goyal et al., 2019; Altan-Bonnet et al., 2020; Handel et al., 2020). The classification of such models includes four complementary levels with emphasis, respectively, on (i) human or animal populations [see, e.g., the articles by Gao et al. (2019) and Fabricius and Maltz (2020), and references therein], (ii) populations of viruses and cells [reviewed in Bocharov et al. (2018b), Smith (2018), Goyal et al. (2019), and Handel et al. (2020)], (iii) interplay of intracellular kinetic steps [reviewed by Yin and Redovich (2018) and Zhdanov (2018)], and (iv) mechanistic details of single steps [reviewed by Jefferys and Sansom (2019) and Altan-Bonnet et al. (2020)]. The corresponding models are primarily temporal. The development of spatio-temporal models pertaining to categories (ii) and (iii) is often complicated due to limited information about how viruses spread within the complex tissues environments of living organisms [such studies are briefly reviewed, e.g., by Sewald et al. (2016)] and what happens inside cells [reviewed by Yin and Redovich (2018)].

Herein, we focus on developing a mathematical framework to describe spatio-temporal aspects of the initial phase of viral infection within the scope of category (ii), i.e., taking virus and cell populations into account. At this level, existing spatio-temporal models are usually aimed at human infections and are constructed by complementing the corresponding temporal models with terms describing the Fickian diffusion of virions in combination with the Neumann (no flux) boundary conditions that do not account for flow in the medium. The first models of this category were, to our knowledge, proposed fifteen years ago by Funka et al. (2005) and Wang and Wang (2007). More recent treatments are described in articles by Bocharov et al. (2018a), Bocharov et al. (2019), Huang et al. (2019), Tang et al. (2019), Yang and Wang (2019), Elaiw and Al Agha (2020), Elaiw et al. (2020), Segredo-Otero and Sanjuan (2020), Tadmon and Foko (2020), Wang and Chen (2020) and Wang et al. (2020). The focus in all these studies was primarily on analyzing the propagation of an infection front [reviewed in Sec. 6 of the book by Bocharov et al. (2018b)] rather than on the start of an infection. By contrast, the mathematical analysis that we develop in this work is aimed at studying the initiation of an infection under flow conditions with diffusion. This scenario is of interest from various

* Corresponding author at: Boreskov Institute of Catalysis, Russian Academy of Sciences, Novosibirsk 630090, Russia.
E-mail address: zhdanov@chalmers.se (V.P. Zhdanov).

https://doi.org/10.1016/j.biosystems.2020.104184
Received 27 April 2020; Received in revised form 7 June 2020; Accepted 7 June 2020
Available online 9 June 2020

perspectives. For example, there is growing evidence that contaminated food and liquids can act as transmission vehicles, whereby the infection of humans and animals often occurs via the consumption of virion-containing food or liquids. In such cases, food and liquid move along and are processed in the intestines, and the initial phase of infection may include the interaction of virions with host cells forming the mucosal layer there. In our model, some of these cells are assumed to be infected by virions and generate new virions under suitable conditions that contribute to growth of the virion population.

Concerning the validation of the model, we add that now it is well-established that foodborne viruses such as norovirus and hepatitis A virus cause infections in humans (Koopmans et al., 2002; Rodriguez-Lazaro et al., 2012). More recently, and in the motivation of our model, there has been growing attention to the role that virion-containing animal feed, feed ingredients, and liquids play in transmitting viruses such as African Swine Fever virus (ASFv) and Porcine Epidemic Diarrhea virus (PEDv) [reviewed by Dee et al. (2016), Boklund et al. (2018), Gordon et al. (2019), and Jones et al. (2019)]. In particular, ASFv is now considered to be one of the most devastating viral infections affecting pigs and wild suids due to the lack of an effective vaccine or antiviral treatment [reviewed by Dixon et al. (2013), Costard et al. (2013), Guinat et al. (2016), Karger et al. (2019), Simoes et al. (2019), and Mason-D'Croz et al. (2020)]. Despite recent progress in characterizing the structure and function of ASFv *in vitro* (including proteomics and replication cycle aspects), there remain limited mechanistic insights into function *in vivo* (Karger et al., 2019; Simoes et al., 2019). In the context of our study, it is of interest to note that there is evidence that the consumption of contaminated feed and liquids is a key transmission route among domestic pigs while direct transmission through close contacts can also be operative (Guinat et al., 2016; Niederwerder et al., 2019). Our results clarify one of the related infection scenarios and also establish a mathematical framework to determine how feed pathogen mitigation might reduce the infection probability of an animal that consumes contaminated feed.

Concerning the novelty of our model in the context of ASFv, we note that now there are a few ASFv-related kinetic models (Barongo et al., 2016; Vergne et al., 2016; Halasa et al., 2018; O'Neill et al., 2020). In the framework of the classification above, they belong to category (i). For example, the most recent temporal model proposed by O'Neill et al. (2020) is based on the division of pigs into four groups including those which are, respectively, uninfected and susceptible to infection, infected and able to transmit the virus, survived, and dead. Each of the first three groups is divided into two subgroups (young and mature). Thus, there are seven equations for the corresponding populations. With these ingredients, the model allowed the authors to assess disease control strategies. In contrast, our model belongs to category (ii) and accordingly is complementary to the above-mentioned models.

Our presentation below is divided into five sections. First, we recall how the initiation of viral infections is described within the framework of the standard temporal model (Section 2). Second, we complement this model by incorporating terms to describe the flow of a feed-containing medium and the diffusion of virions, and present the corresponding analytical results in the case when the kinetic parameters are independent of the coordinate (Section 3). Third, we show the results of numerical calculations performed without and with the dependence of the kinetic parameters on the coordinate along the infected region (Section 4). Fourth, we briefly discuss and illustrate how the function of feed additives used in order to suppress the infection can be described (Section 5). Finally, we outline our main conclusions (Section 6).

2. Standard temporal model

The minimal "standard" (or "basic") temporal model of viral infection operates with the concentrations (or populations) of target and infected cells and virions, $C_*(t)$, $C(t)$, and $c(t)$ (Perelson, 2002; Smith, 2018). Mathematically, it can be formulated as

$$\frac{dC_*}{dt} = w - \mu C_* - kcC_*, \tag{1}$$

$$\frac{dC}{dt} = kcC_* - \kappa C, \tag{2}$$

$$\frac{dc}{dt} = rC - \gamma c + J, \tag{3}$$

where w and J are the supply rates, μ, κ, and γ are the death (or elimination) rate constants, k is the infection rate constant, and r is the virion-production rate constant. A slightly extended version of this model can be obtained by dividing the population of infected cells into two subpopulations staying in the eclipse and active phases, respectively (Smith, 2018).

In reality, viral infection is accompanied by the activation of the immune system. This means that the virion-elimination rate constant, γ, increases with increasing time. In the standard model, γ is considered to be constant. This approximation corresponds to the initial phase of infection. We are interested in this phase and accordingly accept the standard model. Aiming at this phase, we can simplify the model further by assuming $C(t) \ll C_*(t)$ and neglecting the dependence of C_* on time in Eq. (2), i.e., by replacing C_* by $C_*(0)$. Including then $C_*(0)$ into k, i.e., replacing $kC_*(0)$ by k, we rewrite Eq. (2) as

$$\frac{dC}{dt} = kc - \kappa C, \tag{4}$$

In this approximation, Eq. (1) is not needed, and we can operate only with Eqs. (3) and (4).

The types of kinetics predicted by the standard model for the initial phase of infection can be clarified by illustrating its prediction in the steady-state case. In this case, Eq. (4) yields

$$C = (k/\kappa)c, \tag{5}$$

With this relation, Eq. (3) is reduced to

$$(kr/\kappa)c - \gamma c + J = 0, \quad \text{or} \quad c = \kappa J/(\gamma\kappa - kr). \tag{6}$$

The latter expression for the virion concentration indicates that the steady-state regime is possible provided

$$\gamma\kappa > kr. \tag{7}$$

If this condition is not fulfilled, the growth of the populations of infected cells and virions is predicted to be exponential. This can be proved by calculating the eigenvalues corresponding to Eqs. (3) and (4),

$$\lambda_{1,2} = -(\gamma + k)/2 \pm [(\gamma + k)^2/4 - \gamma\kappa + kr]^{1/2}. \tag{8}$$

The kinetics predicted by Eqs. (3) and (4) contain $\exp(\lambda_1 t)$ and $\exp(\lambda_2 t)$. If $\gamma\kappa < kr$, we have $\lambda_1 > 0$, and accordingly the growth is exponential.

3. Standard model with flow and diffusion

Bearing in mind the initiation of viral infection occurring via consumption of contaminated feed, we add the spatial ingredients into the model described above (Section 2). In particular, we again neglect the dependence of the concentration of the target cells on time, include this concentration into the infection rate constant [as in (4)], and operate with the concentrations of infected cells and virions, $C(x,t)$ and $c(x,t)$ (x is the coordinate along the intestine). More specifically, we consider that the cells are immobile and describe infected cells by using the equation apparently identical to (4), i.e.,

$$\frac{\partial C}{\partial t} = kc - \kappa C. \tag{9}$$

The difference between Eqs. (4) and (9) is that the former is temporal (i.e., c depends only on time) while the latter is spatio-temporal (i.e., c depends on time and the coordinate along the intestine). To describe

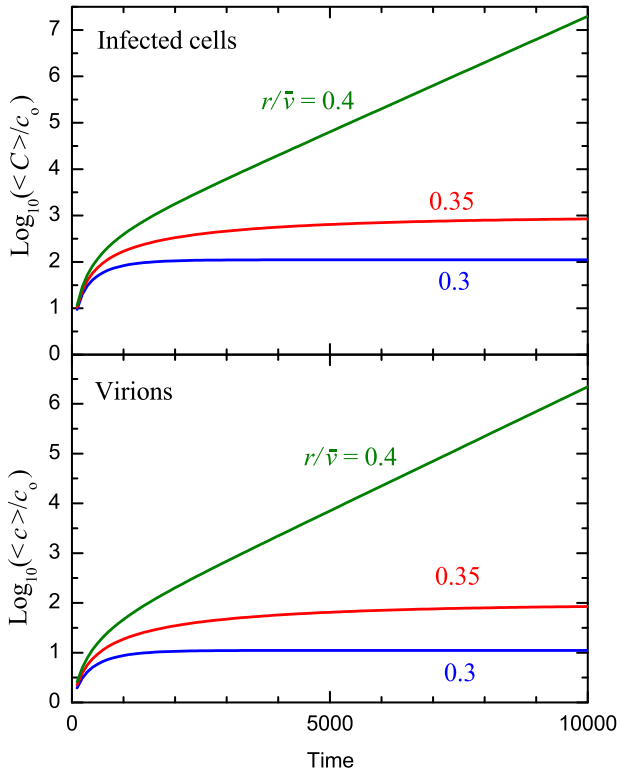

Fig. 1. Logarithm of the normalized average populations of virions and infected cells as a function of dimensionless time, $\bar{\nu}t$, for $r/\bar{\nu} = 0.3$, 0.35, and 0.4. The other parameters are given in the text. With these parameters, the model predicts transition to the steady-state regime for $r/\bar{\nu} = 0.3$ and 0.35 and exponential growth of the populations for $r/\bar{\nu} = 0.4$.

virions, we omit J in Eq. (3) and complement it by the terms taking medium flow and virion diffusion into account, i.e.,

$$\frac{\partial c}{\partial t} = rC - \gamma c - \upsilon\frac{\partial c}{\partial x} + D\frac{\partial^2 c}{\partial x^2}, \tag{10}$$

where υ is the flow rate, and D is the diffusion coefficient. The rate constants in these equations have the same meaning as in (3) and (4).

Concerning the concentrations, C and c, used in Eqs. (9) and (10), we notice that in general concentration can be defined as a number of species per unit volume, surface area, or length. In the case under consideration, C and c can be defined as the number of infected cells and virions per unit surface area and volume of the intestine, respectively. Alternatively, both these concentrations can be defined as the number of species per unit length of the intestine. The latter definition is slightly preferable and employed below, because it allows us to simplify the presentation of the results by normalizing C and c to one properly chosen concentration.

Feed moves along and is processed in the intestine. This means that the conditions for the virion activity change along the intestine. In other words, the rate constants in Eqs. (9) and (10) depend on x. D can depend on x as well, and if this is the case one should replace $D\partial^2 c/\partial x^2$ in Eq. (4) by $\partial(D\partial c/\partial x)/\partial x$. Below (in Section 4), we illustrate the role of the dependence of the rate constants on x in the kinetics under consideration. The dependence of D on x is neglected, because in reality the role of diffusion is expected to be less important compared to flow, and accordingly we can keep D constant in order to show general trends.

By analogy with macromolecules (e.g., protein) in feed, one can expect that the virions function primarily at a certain length scale, i.e., at $0 \le x \le L$, because further on (at $x > L$) their degradation is rapid and their concentration is negligible. Following this line, we solve Eqs. (9) and (10) at $0 \le x \le L$.

Mathematically, the structure of Eqs. (9) and (10) is similar to that used in chemical engineering in order to describe heterogeneous catalytic reactions occurring in a plug-flow reactor with dispersion (Mann, 2009). The terms describing the reaction steps in Eqs. (9) and (10) and the corresponding kinetics are, however, qualitatively different compared to those inherent for heterogeneous catalysis. In particular, the exponential growth is not typical for heterogeneous catalysis. For this reason, the available conventional results of the analysis or the reaction kinetics in a plug-flow reactor with dispersion are not directly applicable in our case.

With the reservation above, we can, however, notice that by analogy with chemical engineering [see, e.g., the discussion by one of us (Zhdanov, 2020)], Eq. (10) can be solved with different boundary conditions. One of the options is to use the Dirichlet boundary conditions implying the concentration of virions at boundaries to be fixed e.g. as

$$c(0,t) = c_o \quad \text{and} \quad c(L,t) = 0, \tag{11}$$

where c_o is the inlet concentration in the feed. The meaning of the former boundary condition is obvious. Concerning the latter boundary condition, it can be valid e.g. in the situations when the virion degradation at $x > L$ rapid and their concentration is there negligible.

Alternatively, one can employ at $x = 0$ the Danckwerts boundary condition implying that the total virion flux,

$$F = \upsilon c - D\frac{\partial c}{\partial x}, \tag{12}$$

is fixed. The discussion of this boundary condition in the context of chemical engineering is given by one of us (Zhdanov, 2020). In our present context, as we have already noticed, the role of diffusion is expected to be less important compared to flow. In this limit, the Dirichlet and Danckwerts boundary conditions are nearly equivalent. With this reservation, we use the Dirichlet boundary conditions in our analysis below, because the corresponding analytical results are somewhat simpler. In particular, we operate with constant inlet concentration. Practically, this means that the feed-mediated supply of virions takes place over a long period. For short periods, the use of the viral dose (or, in other words, viral uptake) might be preferable.

The suitable initial conditions for Eqs. (9) and (10) are as follows

$$C(x,0) = 0 \quad \text{and} \quad c(x,0) = 0. \tag{13}$$

For analytical and numerical calculations, it is convenient to use the dimensionless coordinate, normalize the flow velocity and diffusion coefficient,

$$\bar{x} = x/L, \quad \bar{\upsilon} = \upsilon/L, \quad \text{and} \quad \bar{D} = D/L^2, \tag{14}$$

and rewrite Eq. (10) and conditions (11) and (13), respectively, as

$$\frac{\partial c}{\partial t} = rC - \gamma c - \bar{\upsilon}\frac{\partial c}{\partial \bar{x}} + \bar{D}\frac{\partial^2 c}{\partial \bar{x}^2}, \tag{15}$$

$$c(0,t) = c_o \quad \text{and} \quad c(1,t) = 0, \tag{16}$$

$$C(\bar{x},0) = 0 \quad \text{and} \quad c(\bar{x},0) = 0. \tag{17}$$

Then, Eqs. (9) and (15) can be solved analytically or numerically provided the rate constants are independent of x or numerically provided the rate constants depend x.

As in the case of the temporal model (Section 2), it is instructive first to treat analytically the steady-state situation with $C = (k/\kappa)c$ [cf. Eq. (5)]. With this relation, Eq. (15) is reduced to

$$(kr/\kappa)c - \gamma c - \bar{\upsilon}\frac{\partial c}{\partial \bar{x}} + \bar{D}\frac{\partial^2 c}{\partial \bar{x}^2} = 0. \tag{18}$$

The solution of this equation with conditions (16) is given by

$$\frac{c}{c_o} = \frac{\exp(\eta_1\bar{x}) - \exp(\eta_1 - \eta_2 + \eta_2\bar{x})}{1 - \exp(\eta_1 - \eta_2)}, \tag{19}$$

where

$$\eta_{1,2} = \frac{\bar{\upsilon}}{2\bar{D}} \pm \left[\left(\frac{\bar{\upsilon}}{2\bar{D}}\right)^2 - \frac{\beta}{\bar{D}}\right]^{1/2} \tag{20}$$

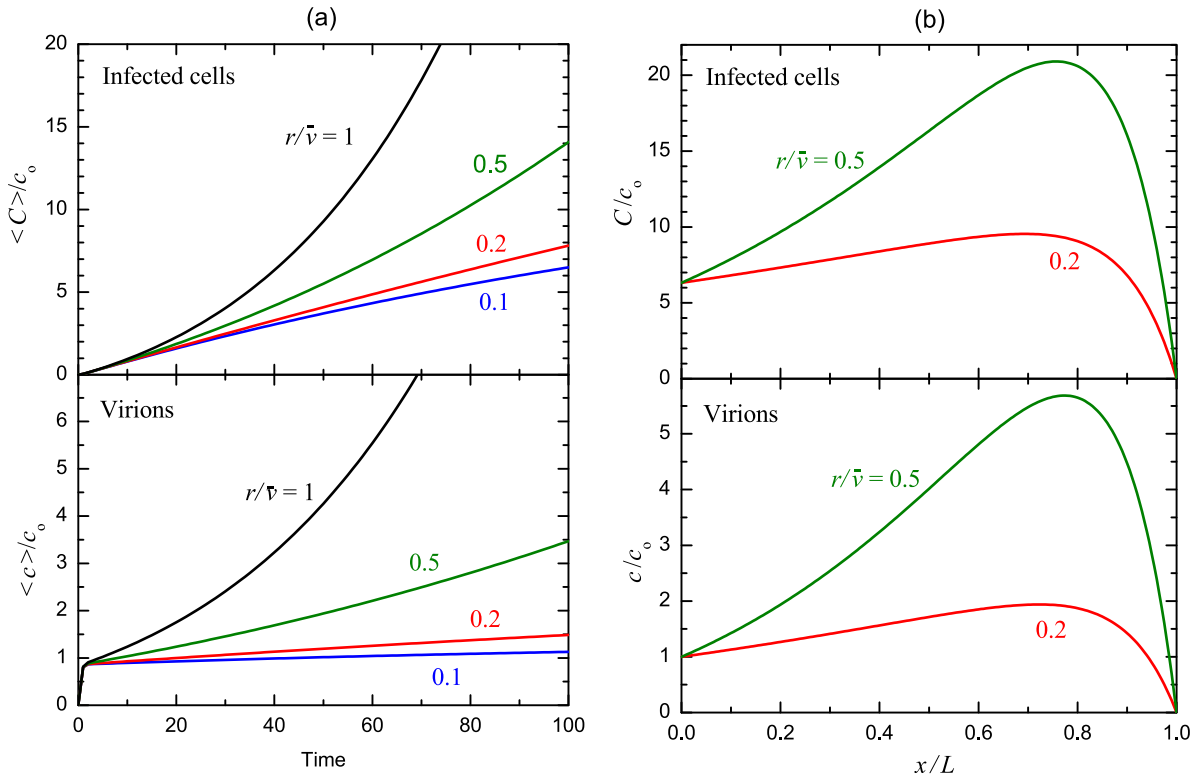

Fig. 2. (a) Normalized average populations of virions and infected cells as a function of dimensionless time, $\bar{v}t$, for $r/\bar{v} = 0.1$, 0.2, 0.5, and 1 (the other parameters are given in the text). (b) Distribution of virions and infected cells along the infection region in the end (at $\bar{v}t = 100$) of the runs with $r/\bar{v} = 0.2$ and 0.5.

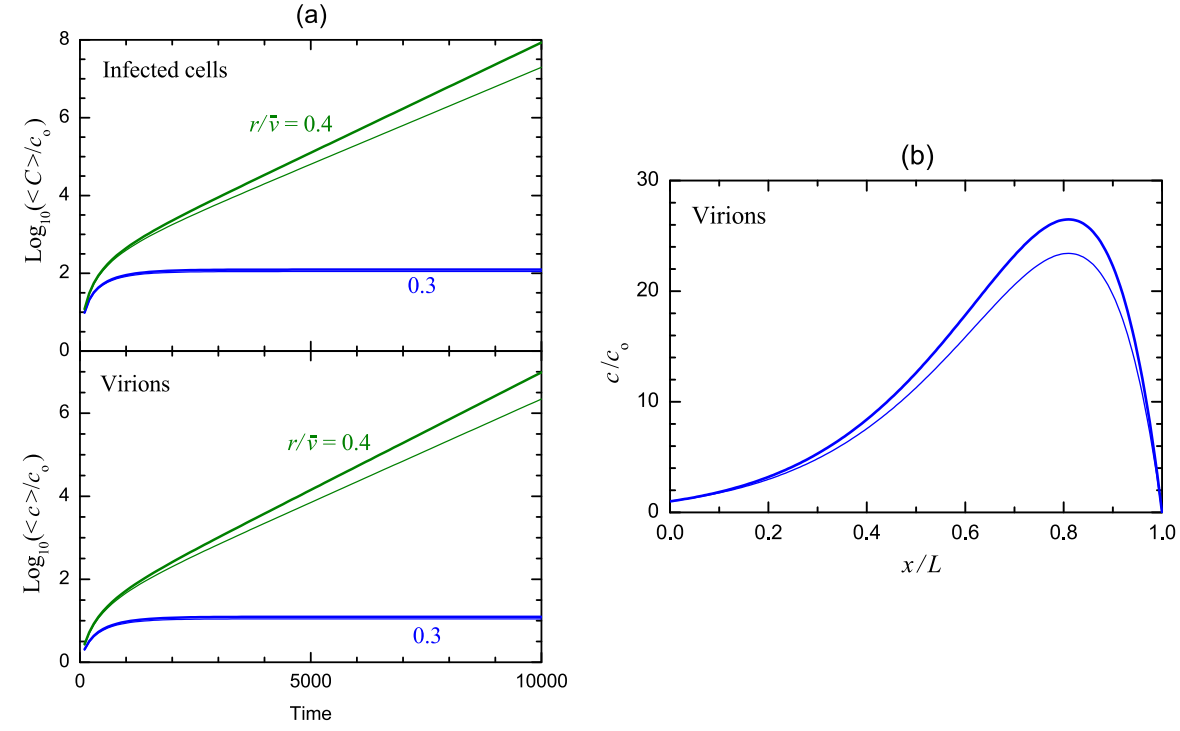

Fig. 3. (a) Normalized average populations of virions and infected cells as a function of dimensionless time, $\bar{v}t$, for $r/\bar{v} = 0.3$ and 0.4 (the other parameters are given in the text). (b) Distribution of virions along the infection region in the end (at $\bar{v}t = 10^4$) of the runs with $r\bar{v} = 0.3$. In both panels, the results obtained by including the dependence of the virion elimination rate constant on the coordinate along the infection region [Eq. (26)] are shown by thick lines. The thin lines correspond to the case when this dependence is neglected. Note that the average populations of virions are nearly equal in these cases so that the corresponding thick and thin lines are hardly distinguishable.

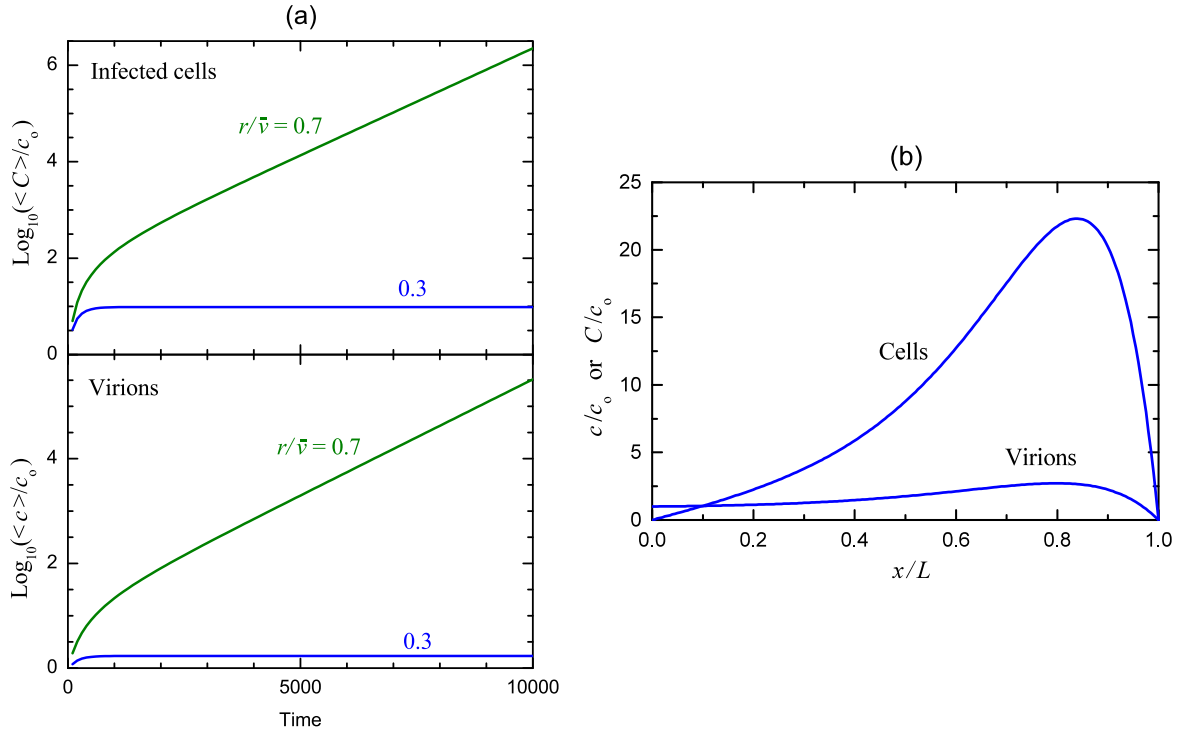

Fig. 4. (a) Normalized average populations of virions and infected cells as a function of dimensionless time, $\bar{v}t$, for $r/\bar{v} = 0.3$ and 0.7 (the other parameters are given in the text). (b) Distribution of virions and infected cells along the infection region in the end of the runs (at $\bar{v}t = 10^4$) shown in panel (a) for $r/\bar{v} = 0.3$. These results were obtained by including the dependence of the cell-infection rate constant on the coordinate along the infection region [Eq. (27)].

and

$$\beta \equiv kr/\kappa - \gamma. \tag{21}$$

If $\beta < \bar{v}^2/4\bar{D}$, η_1 and η_2 are real and expression (19) can be used directly. If $\beta > \bar{v}^2/4\bar{D}$, η_1 and η_2 are complex and can be represented as

$$\eta_{1,2} = b_1 \pm ib_2, \tag{22}$$

where

$$b_1 \equiv \frac{\bar{v}}{2\bar{D}} \quad \text{and} \quad b_2 \equiv \left[\frac{\beta}{\bar{D}} - \left(\frac{\bar{v}}{2\bar{D}}\right)^2\right]^{1/2}. \tag{23}$$

With this specification, expression (19) can be rewritten as

$$\frac{c}{c_o} = \frac{\exp(b_1\bar{x})\sin[b_2(1-\bar{x})]}{\sin(b_2)}. \tag{24}$$

The stability of the steady-state solution [(19) and (24)] of Eqs. (9) and (15) can be identified by calculating the corresponding eigenvalues. In particular, our analysis indicates that the solution is stable provided

$$\beta < \bar{v}^2/4\bar{D} + \bar{D}\pi^2 \quad \text{or} \quad kr/\kappa - \gamma < \bar{v}^2/4\bar{D} + \bar{D}\pi^2. \tag{25}$$

If this condition is not fulfilled, the model predicts exponential growth. Comparing conditions (7) and (25), we conclude that the flow and diffusion extend the domain of applicability of the steady-state solution. Mechanistically, these processes contribute to the removal of virions from the region under consideration ($0 \le x \le L$) and accordingly help to keep infection under control.

4. Numerical calculations

To integrate Eqs. (9) and (15) numerically, we first consider that the rate constants are independent of x and normalize them and $\bar{D}$ to $\bar{v}$. The corresponding calculations were performed by employing the conventional discrete scheme with normalized (dimensionless) parameters $k/\bar{v} = 0.1$, $\kappa/\bar{v} = 0.01$, $\gamma/\bar{v} = 0.1$, and $\bar{D}/\bar{v} = 0.1$, and dimensionless time, $\bar{t} = \bar{v}t$. The normalized virion-production rate constant, $r/\bar{v}$, was used as a governing parameter. According to condition (25), the model predicts in this case the transition to a stable steady state provided $r/\bar{v} < 0.36$. For $r/\bar{v} > 0.36$, the growth of the populations of virions and infected cells is exponential. These regimes are illustrated in Figs. 1 and 2(a) by showing the average populations of virions and infected cells,

$$\langle c\rangle = \int_0^L c\,dx/L \quad \text{and} \quad \langle C\rangle = \int_0^L C\,dx/L,$$

for long and short runs up to $\bar{v}t = 10^4$ and $\bar{v}t = 10^2$, respectively. Typical distributions of virions and infected cells in the end of the latter runs are exhibited in Fig. 2(b). For both regimes, the distributions are similar. In particular, there is a maximum shifted to the right. This feature is related with relatively slow diffusion of virions.

Two examples of the kinetics calculated with the dependence of one of the rate constants on x are shown in Figs. 3 and 4. In the first example (Fig. 3), we consider that the virion elimination rate constant increases with increasing x as

$$\gamma = \gamma_* x/L, \tag{26}$$

where γ_* is the corresponding maximum value. To illustrate the role of this factor, we used $\gamma_*/\bar{v} = 0.1$. This value is the same as that employed for $\gamma/\bar{v}$ in the calculations presented in Fig. 1. The other parameters were fixed also as those used to construct in Fig. 1. With these parameters, the kinetics and virion and infected-cell distributions calculated with and without the dependence of γ on x are nearly the same. This can be explained by relatively rapid removal of virions from the infection domain ($0 \le x \le 1$) due to flow and diffusion. This channel is more efficient than the conventional elimination, and accordingly the details of the conventional elimination are not important.

In the second example (Fig. 4), we consider that the cell-infection rate constant increases with increasing x as

$$k = k_* x/L, \tag{27}$$

where k_* is the corresponding maximum value. By analogy with the first example, this value was chosen to be the same ($k_*/\bar{v} = 0.1$) as that employed for $k/\bar{v}$ in the calculations presented in Fig. 1, and the other parameters were fixed as in the case of Fig. 1 as well. With these parameters, the shape of the kinetics and the virion and infected-cell distributions calculated with and without the dependence of k on x are similar, but the transition to the exponential growth takes place at much larger values of the governing parameter, $r/\bar{v} > 0.6$, than in the case when k is constant (Fig. 1 with $r/\bar{v} > 0.36$).

In addition, we performed calculations in the case when both γ and k depend on x as described above. As expected, the corresponding kinetics are close to those shown in Fig. 4 (not shown).

5. Effect of virus-mitigating feed additives

The model under consideration can be easily extended in various directions. In particular, it can be used directly or with modifications in order to describe e.g. the role of feed additives that can inhibit virus in the feed in order to reduce the chance of infection occurring in animals that consume the feed [such additives employed in the animal agriculture sector are reviewed by Jackman et al. (2020a,b)]. At the simplest level, one can e.g. consider that the viral elimination rate constant depends on the concentration of the additive, c_a,

$$\gamma = \gamma_\circ + Ac_a, \tag{28}$$

where $\gamma_\circ$ is the value corresponding to the additive-free case, and A is a constant. Then, the model can be used directly by considering c_a (or $Ac_a/\bar{v}$) to be a governing parameter. This choice is reasonable provided that an additive is used for a long period (for short periods, the additive dose can be employed). Alternatively, one can consider that c_a depends on the coordinate and complement Eqs. (9) and (10) [or (15)] by the corresponding equation that can be constructed by analogy with Eq. (10).

In this section, we use the former approach including Eqs. (9), (15), and (28). To describe the system without feed additive ($c_a = 0$), we choose the coordinate-independent parameters ($k/\bar{v} = 0.1$, $\kappa/\bar{v} = 0.01$, $r/\bar{v} > 0.5$, $\gamma_\circ/\bar{v} = 0.1$, and $\bar{D}/\bar{v} = 0.1$) so that the populations of virions and infected cells grow exponentially (Fig. 5). Then, $Ac_a/\bar{v}$ is employed as a governing parameter. The corresponding kinetics were calculated for $Ac_a/\bar{v} = 0.01$, 0.1, 1, and 10 (Fig. 5). For $Ac_a/\bar{v} = 0.01$, the effect of an additive on the evolution of infection is predicted to be practically negligible, so that the corresponding kinetics are not distinguishable from those obtained with $c_a = 0$ (not shown). If $Ac_a/\bar{v} = 0.1$ and 1, the effect of an additive on the kinetics is relatively weak and strong, respectively, and, in both cases, the growth remains exponential. For $Ac_a/\bar{v} = 10$, the system reaches a steady state with small populations of virions and infected cells. In other words, this means that the exponential growth is suppressed, and the infection is under control.

6. Conclusion

The initiation of viral infection can be described in the framework of the standard temporal model. We have extended this model by including spatio-temporal aspects that capture important elements of viral infection. Our attention has been focused on the initiation of infection of immobile cells by virions under flow conditions with diffusion. The effects of feed additives used to mitigate viral pathogens and curb disease transmission have also been briefly discussed. The corresponding kinetics have been calculated with the parameters independent of the coordinate as well as with the coordinate-dependent parameters. As in the temporal case, the spatio-temporal model predicts either the transition to a steady state or exponential growth of the populations of virions and infected cells. The spatial distributions of these species are similar in both these regimes. In particular, the maximums of the populations are shifted to the upper boundary of the infected region. In addition, our calculations illustrate how virus-mitigating feed additives can influence the initiation of infection. Our present analysis is focused on the case when the virus supply is steady. The model can, however, be used to describe periodic exposures of virus-containing feed as well.

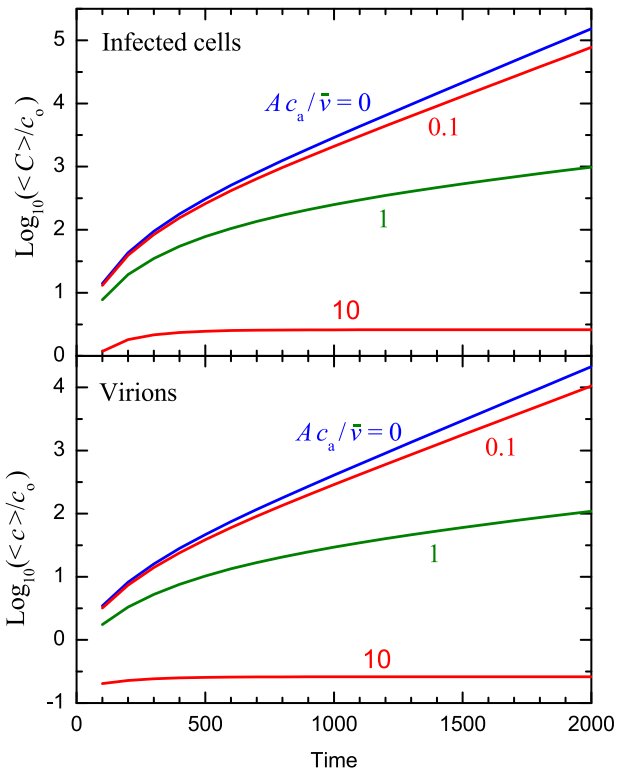

Fig. 5. Logarithm of the normalized average populations of virions and infected cells as a function of dimensionless time, $\bar{v}t$, for $Ac_a/\bar{v} = 0$, 0.1, 1, and 10. The other parameters are given in the text. With these parameters, the model predicts exponential growth of the populations for $Ac_a/\bar{v} = 0$, 0.1, and 1 and transition to the steady-state regime with small populations of virions and infected cells for $Ac_a/\bar{v} = 10$.

In our calculations, we employed normalized dimensionless parameters. This has allowed us to illustrate general trends. From the perspective of applications, it might be of interest to know the scale of the parameters without normalization. In the ASFv-aimed models of category (i) (according to the classification given in the Introduction), the scale of the parameters is already known (Barongo et al., 2016; O'Neill et al., 2020). For the ASFv-aimed models of our category (ii), the related experimental data are, however, still scarce and not sufficient for reliable estimates of the parameters we need.

The model employed is generic and helps to understand the specifics of one of the scenarios of the initiation of viral infection. Thus, the results presented are of interest in the context of theoretical virology and outline the basic steps that can be used to analyze real-life infection cases such as ASFv outbreaks, especially as more mechanistic information becomes available about viral infections in such cases. Some of the diffusion- and flow-related elements of our analysis can be useful, as already mentioned in the Introduction, for constructing the kinetic models aimed at norovirus and hepatitis A infections. These elements are also relevant in other cases including e.g. such respiratory infections as influenza and currently active COVID-19 in which cases the supply of virions is mediated by air flow and often occurs by means of μm-sized water droplets containing virions (Stadnytskyi et al., 2020).

Declaration of competing interest

The authors declare that they have no known competing financial interests or personal relationships that could have appeared to influence the work reported in this paper.

Acknowledgment

This work was supported by the National Research Foundation of Korea (NRF) grant funded by the Korean government (MSIT) (No. 2020R1C1C1004385).

References

Altan-Bonnet, G., Mora, T., Walczak, A.M., 2020. Quantitative immunology for physicists. Phys. Rep. 849, 1–83.
Barongo, M.B., Bishop, R.P., Fevre, E.M., Knobel, D.L., Ssematimba, A., 2016. A mathematical model that simulates control options for African swine fever virus (ASFV). PLoS One 11, e0158658.
Bocharov, G., Meyerhans, A., Bessonov, N., Trofimchuk, S., Volpert, V., 2018a. Interplay between reaction and diffusion processes in governing the dynamics of virus infections. J. Theoret. Biol. 457, 221–236.
Bocharov, G., Meyerhans, A., Bessonov, N., Trofimchuk, S., Volpert, V., 2019. Modelling the dynamics of virus infection and immune response in space and time. Int. J. Parallel Emerg. Distrib. Syst. 34, 341–355.
Bocharov, G., Volpert, V., Ludewig, B., Meyerhans, A., 2018b. Mathematical Immunology of Virus Infections. Springer, Cham.
Boklund, A., et al., 2018. Epidemiological analyses of African swine fever in the European Union (November 2017 until November 2018). EFSA J. 161, e05494.
Costard, S., Mur, L., Lubroth, J., Sanchez-Vizcaino, J.M., Pfeiffer, D.U., 2013. Epidemiology of African swine fever virus. Virus Res. 173, 191–197.
Dee, S., et al., 2016. Modeling the transboundary risk of feed ingredients contaminated with porcine epidemic diarrhea virus. BMC Vet. Res. 12, 51.
Dixon, L.K., Chapman, D.A.G., Netherton, C.L., Upton, C., 2013. African swine fever virus replication and genomics. Virus Res. 173, 3–14.
Elaiw, A.M., Al Agha, A.D., 2020. Analysis of a delayed and diffusive oncolytic M1 virotherapy model with immune response. Nonlinear Anal. Real World Appl. 55, 103116.
Elaiw, A.M., Hobiny, A.D., Al Agha, A.D., 2020. Global dynamics of reaction–diffusion oncolytic M1 virotherapy with immune response. Appl. Math. Comput. 367, 124758.
Fabricius, G., Maltz, A., 2020. Exploring the threshold of epidemic spreading for a stochastic SIR model with local and global contacts. Physica A 540, 123208.
Funka, G.A., Jansen, V.A.A., Bonhoeffer, S., Killingback, T., 2005. Spatial models of virus-immune dynamics. J. Theoret. Biol. 233, 221–236.
Gao, D., van den Driessche, P., Cosner, C., 2019. Habitat fragmentation promotes malaria persistence. J. Math. Biol. 79, 2255–2280.
Gordon, R.K., Kotowski, I.K., Coulson, K.F., Link, D., MacKenzie, A., Bowling-Heyward, J., 2019. The role of non-animal origin feed ingredients in transmission of viral pathogens of swine: A review of scientific literature. Front. Vet. Sci. 6, 273.
Goyal, A., Liao, L.E., Perelson, A.S., 2019. Within-host mathematical models of hepatitis B virus infection: Past, present, and future. Curr. Opin. Syst. Biol. 18, 27–35.
Guinat, C., et al., 2016. Transmission routes of African swine fever virus to domestic pigs: current knowledge and future research directions. Vet. Record 178, 262–267.
Halasa, T., Btner, A., Mortensen, S., Christensen, H., Wulff, S.B., Boklund, A., 2018. Modeling the effects of duration and size of the control zones on the consequences of a hypothetical African swine fever epidemic in Denmark. Front. Vet. Sci. 5, 49.
Handel, A., La Gruta, N.L., Thomas, P.G., 2020. Simulation modelling for immunologists. Nat. Rev. Immun. 20, 186–195.
Huang, K.-S., Shyu, Y.-C., Lin, C.-L., Wang, F.-B., 2019. Mathematical analysis of an HBV model with antibody and spatial heterogeneity. Math. Biosci. Eng. 17, 1820–1837.
Jackman, J.A., Boyd, R.D., Elrod, C.C., 2020a. Medium-chain fatty acids and monoglycerides as feed additives for pig production: Towards gut health improvement and feed pathogen mitigation. J. Anim. Sci. Biotechnol. 11, 44.
Jackman, J.A., Elrod, C.C., Boyd, R.D., 2020b. Fatty Acids and Monoglycerides: Virus-Killing Feed Additives. Feedstuffs (submitted for publication).
Jefferys, E.E., Sansom, M.S.P., 2019. Computational virology: Molecular simulations of virus dynamics and interactions. In: Greber, U.F. (Ed.), Physical Virology, Virus Structure and Mechanics. Springer, Cham, pp. 201–233.
Jones, C.K., Woodworth, J., Dritz, S.S., Paulk, C.B., 2019. Reviewing the risk of feed as a vehicle for swine pathogen transmission. Vet. Med. Sci..
Karger, A., et al., 2019. An update on African swine fever virology. Viruses 11, 864.
Koopmans, M., von Bonsdorff, C.-H., Vinje, J., de Medici, D., Monroe, S., 2002. Foodborne viruses. FEMS Microbiol. Rev. 26, 187–205.
Mann, U., 2009. Principles of Chemical Reactor Analysis and Design: New Tools for Industrial Chemical Reactor Operations. Wiley, Hoboken.
Mason-D'Croz, D., et al., 2020. Modelling the global economic consequences of a major African swine fever outbreak in China. Nat. Food 1, 221–228.
Niederwerder, M.C., et al., 2019. Infectious dose of African swine fever virus when consumed naturally in liquid or feed. Emerg. Infect. Dis. 25, 891–897.
O'Neill, X., White, A., Ruiz-Fons, F., Gortazar, C., 2020. Modelling the transmission and persistence of African swine fever in wild boar in contrasting European scenarios. Sci. Rep. 10, 5895.
Perelson, A.S., 2002. Modelling viral and immune system dynamics. Nat. Rev. Immunol. 2, 28–36.
Rodriguez-Lazaro, D., et al., 2012. Virus hazards from food, water and other contaminated environments. FEMS Microbiol. Rev. 36, 786–814.
Segredo-Otero, E., Sanjuan, R., 2020. The role of spatial structure in the evolution of viral innate immunity evasion: A diffusionreaction cellular automaton model. PLoS Comput. Biol. 16, e1007656.
Sewald, X., Motamedi, N., Mothes, W., 2016. Viruses exploit the tissue physiology of the host to spread in vivo. Curr. Opin. Cell Biol. 41, 81–90.
Simoes, M., Freitas, F.B., Leitao, A., Martins, C., Ferreira, F., 2019. African swine fever virus replication events and cell nucleus: New insights and perspectives. Virus Res. 270, 197667.
Smith, A.M., 2018. Validated models of immune response to virus infection. Curr. Opin. Syst. Biol. 12, 46–52.
Stadnytskyi, V., Bax, C.E., Bax, A., Anfinrud, P., 2020. The airborne lifetime of small speech droplets and their potential importance in SARS-CoV-2 transmission. Proc. Nat. Acad. Sci. USA 117, 11875–11877.
Tadmon, C., Foko, S., 2020. Non-standard finite difference method applied to an initial boundary value problem describing hepatitis B virus infection. J. Diff. Eq. Appl. 26, 122–139.
Tang, S., Teng, Z., Miao, H., 2019. Global dynamics of a reaction–diffusion virus infection model with humoral immunity and nonlinear incidence. Comput. Math. Appl. 78, 786–806.
Vergne, T., Korennoy, F., Combelles, L., Gogin, A., Pfeiffer, D.U., 2016. Modelling African swine fever presence and reported abundance in the Russian Federation using national surveillance data from 2007 to 2014. Spat. Spat.-temp. Epidem. 19, 70–77.
Wang, J., Chen, Y., 2020. Threshold dynamics of a vector-borne disease model with spatial structure and vector-bias. Appl. Math. Lett. 100, 106052.
Wang, K., Wang, W., 2007. Propagation of HBV with spatial dependence. Math. Biosci. 210, 78–95.
Wang, W., Wang, X., Guo, K., Ma, W., 2020. Global analysis of a diffusive viral model with cell-to-cell infection and incubation period. Math. Methods Appl. Sci. 43, 5963–5978.
Yang, J., Wang, X., 2019. Dynamics and asymptotical profiles of an age-structured viral infection model with spatial diffusion. Appl. Math. Comput. 360, 236–254.
Yin, J., Redovich, J., 2018. Kinetic modeling of virus growth in cells. Microbiol. Mol. Biol. Rev. 82, e00066-17.
Zhdanov, V.P., 2018. Initial phase of replication of plus-stranded RNA viruses. Biophys. Rev. Lett. 13, 93–108.
Zhdanov, V.P., 2020. Kinetics of reaction on a single catalytic particle in a fluidic nanochannel. Catal. Lett. 150, 1749–1756.